ELSEVIER

Remote Sensing of Environment

Local Maximum Filtering for the Extraction of Tree Locations and Basal Area from High Spatial Resolution Imagery

Mike Wulder,[*,†] *K. Olaf Niemann,*[†] *and David G. Goodenough*[†,‡]

In this study we investigate the use of local maximum (LM) filtering to locate trees on high spatial resolution (1-m) imagery. Results are considered in terms of commission error (falsely indicated trees) and omission error (missed trees). Tree isolation accuracy is also considered as a function of tree crown size. The success of LM filtering in locating trees depends on the size and distribution of trees in relation to the image spatial resolution. A static-sized 3×3 pixel LM filter provides an indication of the maximum number of trees that may be found in the imagery, yet high errors of commission reduce the integrity of the results. Variable window-size techniques may be applied to reduce both the errors of commission and omission, especially for larger trees. The distribution of the error by tree size is important since the large trees account for a greater proportion of the stand basal area than the smaller trees. An investigation of the success of tree identification by tree crown radius demonstrates the relationship between image spatial resolution and LM filtering success. At an image spatial resolution of 1 m, a tree crown radius of 1.5 m appears to be the minimum size for reliable identification of tree locations using LM filtering. ©*Elsevier Science Inc., 2000*

INTRODUCTION

Local maximum (LM) filtering of high spatial resolution imagery provides a way to isolate and characterize individual trees. High spatial resolution imagery offers foresters an additional source of data for forest inventory compilation, validation, and audit purposes. The ability to directly estimate the location of trees may improve estimates of stand density, volume, basal area, and canopy closure compared to estimates based on lower spatial resolution data. For example, forest stand density has been estimated from lower resolution data (Landsat TM) with an accuracy too low for inventory use, but high enough for regional density characterization (Franklin, 1994; Wu and Strahler, 1994). For high spatial resolution data to be applied in forest inventories, the accuracy and potential limitations need to be addressed. High spatial resolution imagery has recently come to the attention of ecologists interested in forest dynamics at the individual tree level (Warner et al., 1999). The ability to use remotely sensed data to sample large areas and to locate and identify individual trees with unique characteristics may aid ecologists. In this study, we investigate the use of LM filtering in a forestry context.

When remote sensing instruments collect data above a forested landscape, the horizontally continuous surface is digitally partitioned into a grid of pixels. The size and shape of the remotely sensed pixels dictates the amount of the original landscape variance that is captured. Low spatial resolution imagery tends to reduce the variance between pixels through inclusion of a variety of surface cover types within each pixel. Conversely, airborne remote sensing and current (Mangold, 1999) and proposed high resolution satellite instruments (Aplin et al., 1997) partition the surface into smaller pixels and capture a greater amount of the original variance. As a result, high resolution imagery of a forest is composed of contiguous pixel regions, which represent individual trees or clusters of trees (Wulder, 1999). Some of the possible approaches to the detection of individual tree crowns are valley follow-

* Pacific Forestry Centre, Canadian Forest Service, Natural Resources Canada
† University of Victoria, Department of Geography
‡ University of Victoria, Department of Computer Science
Address correspondence to M. Wulder, 506 West Burnside Road, Victoria, BC V8Z 1M5, Canada. E-mail: mwulder@pfc.forestry.ca
Received 20 August 1999; revised 19 January 2000.

655 Avenue of the Americas, New York, NY 10010

0034-4257/00/$–see front matter
PII S0034-4257(00)00101-2

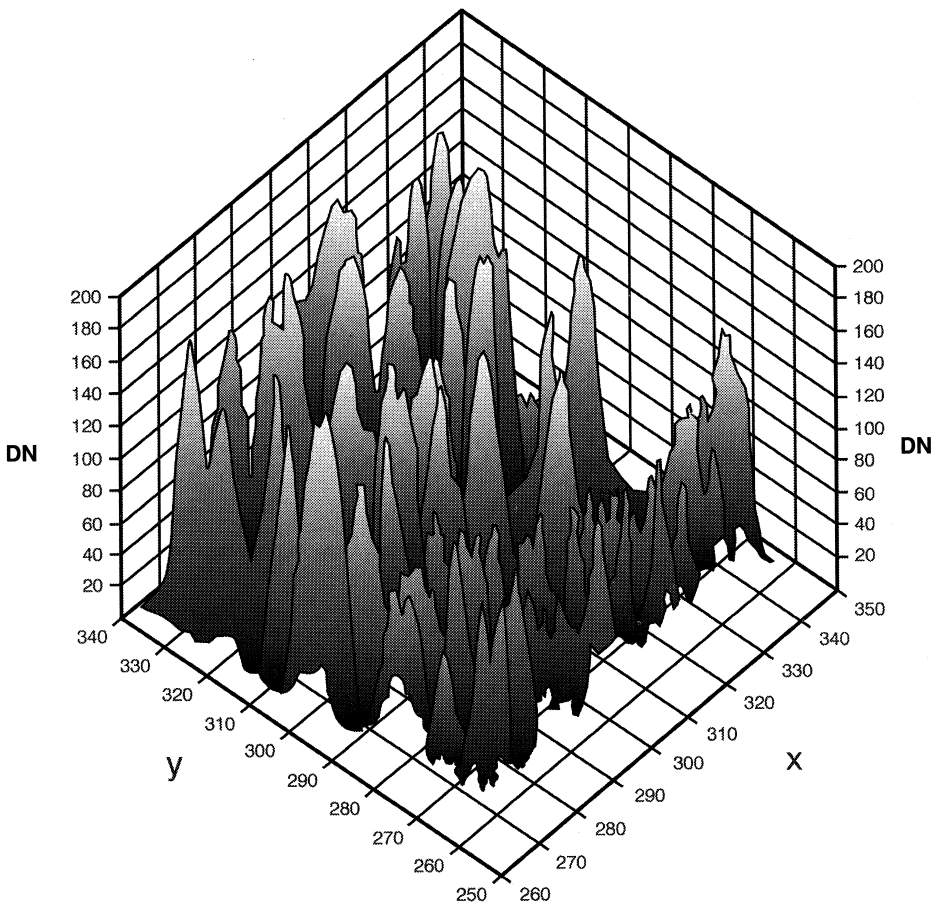

Figure 1. Digital surface of a forest stand. Local maximum reflectance is related to the presence of tree crown centers. This surface was created using an LM filter on 1-m spatial resolution imagery (x and y denoting the pixel/line location of the DNs in the study image).

ing (Gougeon, 1999), radiance peak filtering (Gougeon and Moore, 1988; Gougeon and Moore, 1989; Dralle and Rudemo, 1997; Niemann et al., 1999), edge finding (Pinz, 1999), template matching (Pollock, 1999), morphology (Barbezat and Jacot, 1999), and clustering (Culvenor et al., 1999; Wulder, 1999). The variety of techniques for processing individual trees from high spatial resolution imagery is due to the differing image spatial structure that emerges from the complex relationships between image spatial resolution and forest structural characteristics. For example, at a very high image spatial resolution (≈10 cm) the morphology of individual trees may be detected (Brandtberg, 1997). As the image spatial resolution decreases, the most appropriate image processing technique appears to change from valley following, to radiance peak filtering, to texture, to geometrical optical modeling (Wulder, 1998).

Individual trees may be discerned in medium to densely forested areas on high spatial resolution imagery as regions of high reflectance. For conifers the spatial structure of this reflectance results in a local maximum value found at or near the center of trees (Fig. 1). The structure of this reflectance is related to the contrast between pixels representative of trees and the relative brightness of the background material present. In LM filtering, a window is passed over all pixels in an image to determine if a given pixel is of higher reflectance than all other pixels within the window (Dralle and Rudemo, 1997). Pixels identified as the largest digital number within the window are noted as tree locations. When a window of a fixed size is passed over an image it does not account for the presence of trees with different crown sizes [i.e., static-sized windows do not take into account the object-resolution relationship that exists between the trees (objects) and the image spatial resolution]. The concept of H-resolution, posited by Strahler et al. (1986), presents the relationship between image spatial resolution and image object representation in terms of variance. An H-resolution pixel is spectrally representative of a single object (e.g., tree crown), with a number of similar pixels composing the individual object. As a result, the ability to isolate trees with an LM filter requires an image spatial resolution that is finer than the mean crown size of trees present. Successful recognition of the resolvable trees using LM filtering relies on careful selection of the filter window size. If the selected window is too small, errors of commission occur through selection of nonexistent trees or multiple radiance peaks for an individual tree crown. If the window is too large, errors of omission increase. Observation of changing omission and commission errors as a function of crown radii provides an indication of the relation between tree

size and image resolution required to resolve individual trees with an LM filter.

To address these issues, in this study a variable window was used for the filtering of local maxima. The dynamic allocation of window sizes based on local image spatial structure results in a custom-sized window for each pixel. Franklin et al. (1996) demonstrate the use of semivariance to customize window sizes for use in texture analysis; we apply similar methodology in this study to size windows that are appropriate for the filtering of local peak radiance values. In this study we also investigate a parameter called the "slope break" to compute variable window sizes.

The goal of incorporating spatial information into the determination of window size for LM filtering is to decrease the commission error resulting from the erroneous detection of LM filtering that does not represent trees. Omission error with the LM technique is largely a function of image resolution. Additional tree detection errors may arise through factors such as close proximity of neighboring trees, trees being located under other trees, trees found in shadows, or trees having low spectral contrast with respect to the understory vegetation. As a result, a primary aim when applying LM filters is to maximize the number of legitimate trees found while also minimizing the amount of pixels falsely identified as tree locations. Once the issues impacting the efficacy of LM filtering with fixed and variable window sizes are addressed, the limits of the estimates are investigated, and the implications of using LM-indicated trees in an example operational application are presented. The objectives of this study are to:

- assess the ability to locate trees with 1-m spatial resolution airborne multispectral MEIS-II imagery in different spectral regions (red, infrared, and panchromatic) and with variable and static window sizes;
- analyze the distribution of errors of missed trees (omission) and incorrectly identified trees (commission), in terms of detection technique and forest structure;
- assess the potential of the LM techniques for imagery collected with high spatial resolution satellites;
- address the effects of errors on the computation of stand basal area from LM-located trees; and
- explore the relationship between crown radius and likelihood of selection by an LM filter.

METHODS

Study Area and Ground Plot Data

The Greater Victoria Watershed is located at 48°23′ latitude and 123°41′ longitude, which is northwest of Victoria, British Columbia (Fig. 2). Within this watershed, a 0.72-ha study area with little topographic variability, composed of a 40-year-old plantation and a 150-year-old naturally regenerating mature stand (GVWD, 1991), was selected. The plantation (planted in 1965 and thinned in 1975) is composed of trees ranging in height from 8.6 m to 25 m and is a mixture of Douglas fir (*Pseudotsuga menziesii*) and western red cedar (*Thuja plicata*), while the mature stand contains trees from 140 years to 250 years of age ranging in height from 20 m to 70 m, and is dominated by Douglas fir (Table 1). The 0.72-ha study area was partitioned into 72 grid cells of 10 m by 10 m, within which all trees were measured and located to 0.1 m of precision to allow for the creation of a stem map. In total 209 trees were located with 159 trees in the plantation stand and 50 trees in the mature stand. As part of the fieldwork for Hay and Niemann (1994), crown radius, diameter at breast height (DBH), species type, tree height at crown apex, and height at maximum crown radius were measured. The correlations between field data measurements (Table 2) are high over the full range of the data, yet diminish when considered within each age class. The lower correlations calculated for the stratified data is related to the reduced amount of variance and may indicate the presence of overly influential points when considering the full range of data. Also pres-

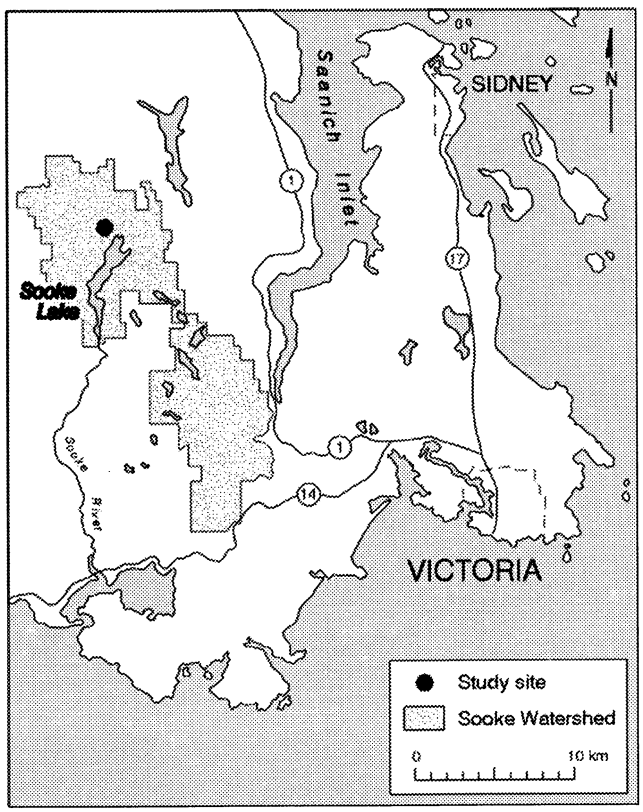

Figure 2. Sooke Watershed study area shown in light gray northwest of Victoria, British Columbia, Canada.

Table 1. Field Survey Summary Statistics for the Complete Field Data Set and Divided by Stand Age

	All (n=*209*)			*Plantation* (n=*159*)			*Mature* (n=*50*)		
	DBH (cm)	*Height (m)*	*Crown Radius (m)*	*DBH (cm)*	*Height (m)*	*Crown Radius (m)*	*DBH (cm)*	*Height (m)*	*Crown Radius (m)*
Mean	37.0	26.0	1.8	22.5	19.3	1.4	85.0	47.6	3.1
Median	24	20.7	1.6	22	19.6	1.4	85.5	49.1	3.1
Minimum	9	8.6	0.7	9	8.6	0.7	33	19.8	1.8
Maximum	158	69.3	4.5	37	25.0	2.3	158	69.3	4.5
Range	149	60.7	3.8	28	16.4	1.6	125	49.4	2.7
Standard deviation	29.6	13.5	0.8	5.2	3.0	0.3	23.2	11.1	0.6

ent in the study site is a dense layer of understory consisting of hemlock (*Tsuga heterophylla*), some red alder (*Alnus rubra*), salal (*Gaultheria shallon*), sword fern (*Polystichum munitum*), Oregon grape (*Mahonia nervosa*) and Oregon beaked moss (*Kindbergia oregana*).

MEIS-II Image Data

The second generation Multi-Detector Electro-Optical Imaging Sensor (MEIS-II) (Till et al., 1983) was flown at an altitude of 1428 m over the study site at 11:30 A.M. PST on 2 September 1993 during the first field campaign of the SEIDAM (System of Experts for Intelligent Data Management) project (Goodenough et al., 1994; Goodenough et al., 1997). The resulting ground pixel size is 1 m, with all images resampled to 720 pixels across track. The raw data were geometrically corrected using British Columbia Ministry of Environment Terrain Resource Information Management (TRIM) digital elevation data with a horizontal accuracy of ±20 m. Solar altitude and azimuth angles at the time of the flight were 52° and 133°, respectively.

The MEIS-II is a push broom scanner with a temperature-stabilized CCD linear array and a spectral range from 380 nm to 1,100 nm. Within the 720-nm spectral range six user-defined, nadir-looking channels (Table 3) may be selected by mounting filters in front of the lens. A panchromatic channel was simulated by averaging the six available channels to summarize the spectral response found over the MEIS-II spectral available range from 432.85 nm to 847.65 nm (Table 3). This enabled a comparison with the 1-m panchromatic image data available on the IKONOS satellite (with a 450-nm to 900-nm panchromatic channel) and forthcoming high spatial resolution satellite sensors (Aplin et al., 1997).

Table 2. Correlations between Field-Collected Data

	All (n=*209*)	*Plantation* (n=*159*)	*Mature* (n=*50*)
DBH and height	0.95	0.58	0.76
DBH and crown radius	0.90	0.73	0.53
Crown radius and height	0.87	0.52	0.44

Variable Window-Size Computation

Semivariance

Variable window sizes are suggested for each pixel location based on an average semivariance range values computed from transects in the eight cardinal directions around each pixel in the image. Digital image semivariance indicates pixel self-similarity over a transect of pixels. Semivariance is a well-understood and frequently applied image processing technique in remote sensing (Curran and Atkinson, 1998). A variogram describes the magnitude, spatial scale, and general form of the variation in a given set of data (Matheron, 1963). Semivariograms provide a means of measuring the spatial dependency of continuously varying phenomena.

A remotely sensed image may be processed for semivariance through the computation of the relationships between pixel pairs. In the case of a transect passing across a remotely sensed image, the digital numbers z of pixel transect x are extracted at regular intervals (where $[x = 1, 2, \ldots, n]$). The relationship between a pair of pixels found h pixels apart, or the "lag" distance, is recorded as the average squared difference between all pixel pairs. The semivariogram, $\gamma(h)$, is a plot of semivariance as a function of lag (Curran and Atkinson, 1998) and can be computed as shown in Eq. (1):

$$\gamma(h)=\frac{1}{2}E[Z(x)-Z(x-h)]^2 \quad (1)$$

Where Z denotes a pixel value at a location x. The lag h indexes the distance between pairs for comparison. In each transect of values there will be $m(h)$ observational pairs separated by the same lag distance h. The value is an estimate of the semivariance and is understood as a measure of dissimilarity between spatially separated pixels (Jupp et al., 1988). For a given lag h, the semivariance is calculated as seen in Eq. (2):

$$\hat{\gamma}(h)=\frac{1}{2m(h)}\sum_{i=1}^{m(h)}[z(x_i)-z(x_i-h)]^2 \quad (2)$$

If there is spatial structure in a given dataset, a semivariogram will reveal that semivariance rises until reaching the "sill," which indicates the maximum variability be-

Table 3. MEIS-II Spectral Channels Available in Data Set

Channel	*Blue*	*Green*	*Green*	*Red*	*Red*[a]	*Infrared*[a]
Wavelength centre (nm)	448	518	553	641	675	875
Mean bandwidth (nm)	30.3	23.9	13.8	37.0	39.5	54.7

[a] Channels used in this study.

tween pixels. The "range" is the number of lags, or distance, to the sill (Curran and Atkinson, 1998). Therefore, within the range spatial dependence between pixel values is indicated. The pixel values at the lag locations greater than the range are understood as spatially independent of values within the range (Lévesque and King, 1996). For this study a bounded semivariogram model is assumed. If an unbounded model is encountered the range is set at the maximum allowable lag location. The maximum allowable lag location is set as one-third (10 pixels) of the total transect length (30 pixels) as the reliability of semivariance [$\gamma(h)$], decreases with increasing lag (h) (Curran and Atkinson, 1998).

To minimize the potential effects of image anisotropy, image semivariance is computed for all eight cardinal directions out from the central pixel, with the average of the eight results stored in a new image channel. Computing an average range value for each pixel in the image reduces problems that arise when attempting to select a representative single transect origin and angle (Wulder et al., 1998). In this research, omnidirectional semivariance is computed for each pixel that is found to be within an edge buffer of 30 pixels. For each transect the semivariance at each lag is stored in an array until the semivariance values cease to increase. The highest lag value, understood to be the sill, provides the lag number to be written to an array to represent the range for that direction. This procedure is followed for all eight directions. The eight directional range values are then averaged and written to file as the range to represent that pixel location. This procedure is applied to all pixels inside the image buffer.

The conversion of semivariance ranges to window sizes requires user intervention (Daley et al., 1998). In Table 4 the conversion lookup table is presented. The semivariance ranges tend to be larger than required for direct conversion to a window size, which is likely due to the semivariance response being a function of the stand structure, not only the individual tree structure. The interpixel variability is limited at a 1-m spatial resolution, particularly in dense homogenous stands, which results in ranges that characterize the stand spatial dependency rather than that of individual trees.

Table 4. Semivariance Range Conversion to Square Window-Size Key in Pixels

Semivariance Range	*Slope Break*	*Window Size*
⩽4	⩽3	3
5,6	4,5	5
⩾7	⩾6	7

Slope Breaks

To overcome the need for user intervention in the determination of optimal window size, "slope breaks" were calculated. Slope breaks are a simple means of measuring the region of dependence around a pixel. Slope breaks are based on the assumption that every tree in an image may be a local maximum. For each pixel in the imagery an omnidirectional set of transects is analyzed from the central pixel to assess the number of pixels until a minimum radiance value is reached. The slope break may also be described as the first inflection point in the gradient of reflectance around the tree. The inflection point may be considered as an edge location. The mean value of the number of pixels to the slope reversal for all eight cardinal directions is used as a custom window size for that pixel. If a pixel's radiance is lower than all surrounding pixels, a value of zero is assigned for the window size. The conversion from slope break value for a pixel to customized window size requires no user intervention (Table 4).

LM Processing

Isolation of the role of window size, spectral channel, threshold filtering, and LM processing of spatial dependence information in the ability to identify individual trees is necessary to address the objectives of this study. Tree crown locations were identified using 11 different LM filter configurations, which are combinations of window sizes, either static or variable square windows with sides of three, five, and seven pixels and the three spectral ranges (red, infrared, and panchromatic). Differing spectral ranges are investigated as the spectral conditions, such as spectral range and interpixel contrast, may relate to LM tree identification success. The variable window sizes assigned to each pixel are based on the semivariance range or local breaks in slope.

Tree crown locations from the different filtering combinations were compared for commission and omission errors to a detailed digital ground survey stem map. For each LM filter configuration, the results are considered in terms of total proportion of trees correctly selected and the proportions of commission and omission errors. The total proportion correct, omission error, and commission error are considered in terms of all trees

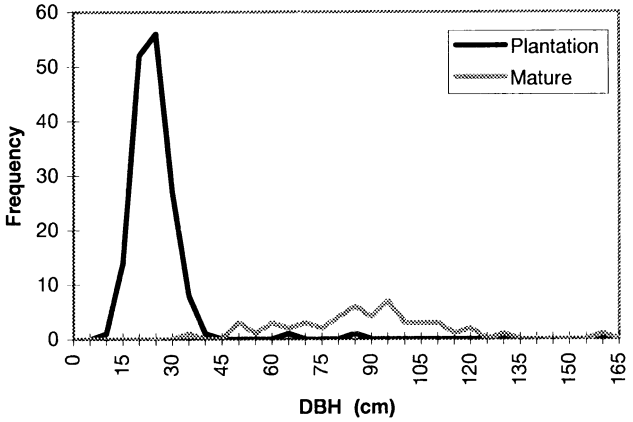

Figure 3. Frequency distribution of field data DBH values for a plantation and a mature natural stand.

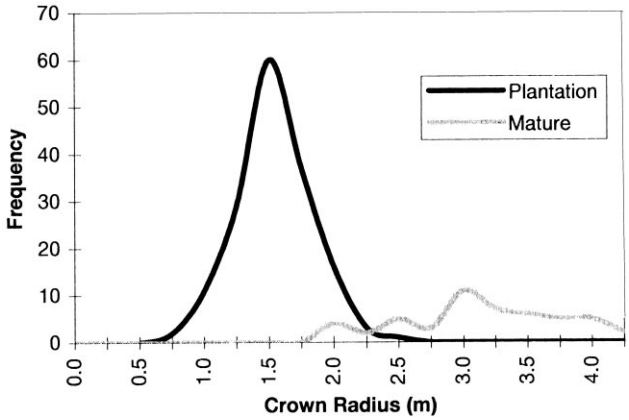

Figure 4. Frequency distribution of field data crown radius values for a plantation and a mature natural stand.

present in the stand and with the stand partitioned into plantation and mature components. Errors of commission and omission are assessed in relation to tree DBHs and crown radii.

The study area is partitioned into plantation and mature components since the tree size distribution in each component is relatively homogeneous. Partitioning the stand into age components that have differing structural characteristics allows assessment of errors of commission and omission in terms of distinct stand structural regimes.

Field measurements of DBH and crown radius were stratified into ranges to accentuate the identification thresholds and their relationship to errors of commission and omission. Based on the distribution of DBH (Fig. 3; Table 1) the trees are partitioned into three ranges: DBH less than 35 cm, DBH from 35 cm to 70 cm, and DBH greater than 70 cm. The majority of the trees in the plantation stand had a DBH lower than 35 cm. The majority of the trees in the mature stand had a DBH over 70 cm. The crown radius ranges are also based on natural breaks in the field data, capturing the structural distinction between the plantation and mature stands. The crown radii are partitioned into six ranges: less than 1 m, 1 m to 1.5 m, 1.5 m to 2 m, 2 m to 3 m, 3 m to 4 m, and greater than 4 m. The majority of the crown radii fall within 1 m to 2 m (Fig. 4). As a result, to better capture the distribution of error by crown radii, this range was divided in half.

RESULTS AND DISCUSSION

Individual Tree Detection

Spectral Region and Filtering Success

Prior to comparison of static to variable window sizes, the performance of the static window sizes must be evaluated. In Table 5 we present the proportion of correct, omitted (missed), and committed (falsely identified) trees for fixed window LM filtering of image spectral data. The 3×3 LM filter represents a superset of all possible LM that may be isolated using a local maximum technique. The 3×3 LM filter finds all local maxima, without regard to any image spatial structure and, as a result, the commission error is generally high. The 3×3 LM filter on both the red and simulated panchromatic ranges correctly located 67% of the trees in both age classes. In an operational application, the detailed field data likely would not be present; in that situation, there would be no way to detect false positives, resulting in an overestimate of stems, which emphasizes the need to minimize commission error.

In Table 5 we also present the performance of the static-sized LM filters in terms of stand age and structure. For a visual presentation of the results see Figure 5. The increase in window size from 3×3 through 5×5 to 7×7 results in increasingly poor results (i.e., more missed trees) for the plantation stand with less of an effect on the mature stand, indicating that data with resolution higher than 1 m are required for small tree detection. Comparison of the younger plantation stand with the naturally regenerating mature stand provides an indication of the object-resolution relationship present. The lower success in identifying field-located trees in the plantation stand in comparison to the mature stand indicates an inability to discern the smaller trees with 1-m data. The maximum of 67% correct overall may be interpreted as a function of the object-resolution relationship.

With a minimum of ≈40% of the plantation trees being missed with LM techniques in this study, it appears that 1-m imagery is too coarse for individual tree crown recognition in a Douglas fir stand with crown radii less that 1.5 m. The mature stand, with an omission level of ≈20%, appears to have a stand structure that is more appropriate for LM filtering of 1-m spatial resolution imagery. The omission error may be interpreted as being largely a function of the image spatial resolution, whereas

Table 5. Results of Fixed and Variable Window-Size LM Filter Processing of Spectral Image Data

	Wavelength										
	Red (675 nm)			*IR (875 nm)*			*PAN (≈448–875 nm)*			*PAN (≈448–875 nm)*	
Window Size	*3×3*	*5×5*	*7×7*	*3×3*	*5×5*	*7×7*	*3×3*	*5×5*	*7×7*	*SVR*	*SB*
ALL (n=209)											
Correct	0.67	0.46	0.31	0.65	0.49	0.28	0.67	0.50	0.30	0.64	0.62
False positive	0.25	0.08	0.04	0.15	0.04	0.02	0.22	0.05	0.02	0.19	0.11
Missed	0.33	0.54	0.69	0.35	0.51	0.72	0.33	0.50	0.70	0.36	0.38
Plantation (n=159)											
Correct	0.61	0.39	0.21	0.60	0.42	0.19	0.62	0.43	0.21	0.60	0.56
False positive	0.08	0.02	0.01	0.03	0.02	0.01	0.05	0.02	0.01	0.05	0.03
Missed	0.39	0.61	0.79	0.40	0.58	0.81	0.38	0.57	0.79	0.40	0.44
Mature (n=50)											
Correct	0.84	0.68	0.62	0.78	0.70	0.58	0.80	0.72	0.60	0.76	0.80
False positive	0.78	0.26	0.16	0.54	0.12	0.06	0.78	0.10	0.08	0.64	0.38
Missed	0.16	0.32	0.38	0.22	0.30	0.42	0.20	0.28	0.40	0.24	0.20

SVR, semivariance range; SB, slope break.

the commission error is related to the occurrence of spurious local maxima unrelated to the reflective characteristics of the crown canopy.

The proportions of trees identified for each spectral channel appear similar for each window size. As expected, the success of tree identification diminishes with increasing window size; further, the larger image objects found in the mature stand are found to have a smaller decrease in success than the plantation stand with smaller image objects. To reduce the redundancy of the results presented, a chi-square analysis was undertaken to assess the statistical variability of the LM filtering results. The results indicated no statistical difference (χ^2 of 9.49, α=0.05, with 4° of freedom) between the LM filtering results generated for each stand (all, plantation, and mature) or at each window size for each spectral range. Based on the lack of a significant difference between the LM filtering on the differing wavelength ranges, the results of a single channel are presented. The simulated panchromatic channel has been selected for further presentation and analysis since satellites currently available and planned for launch in the near future will have similar spatial and spectral configurations (Mangold, 1999; Aplin et al., 1997).

Static versus Variable Window Sizes

Variable window sizes were applied to the LM filtering process in an attempt to reduce the level of commission error, or false positives, by integrating scene spatial structural information. Semivariance range and slope

Figure 5. Example of a variety of LM filtering results. Complete study area within green region, with the plantation stand upper and the mature stand lower. (A) Red with 3×3 LM filter (correct 0.67, commission 0.25, omission 0.33). (B) PAN with SB LM filter (correct 0.62, commission 0.11, omission 0.38).

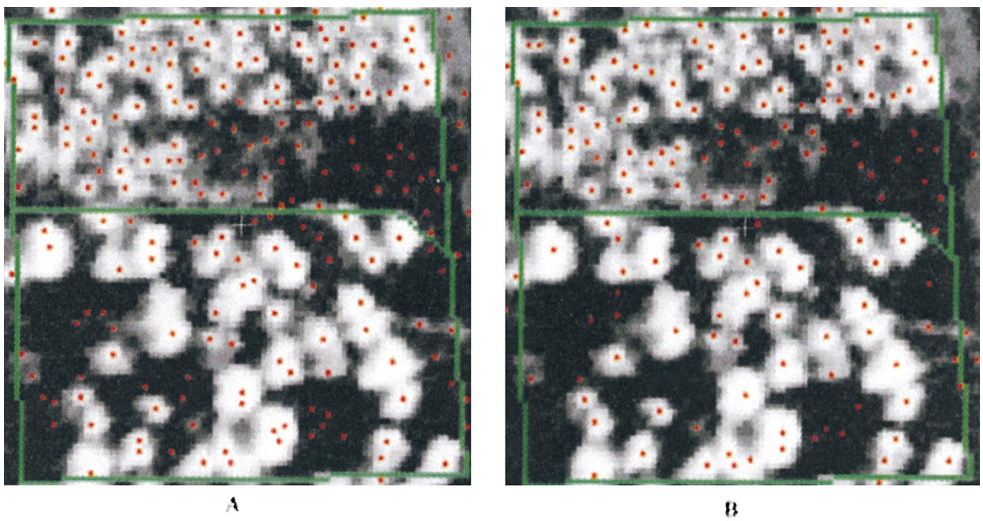

Table 6. Proportion of Trees Correctly Located by DBH Range on Panchromatic Data

	All (n=209)			*Plantation* (n=159)			*Mature* (n=50)		
Portion of Stand DBH range (cm)	*<35* (n=158)	*35–70* (n=14)	*>70* (n=37)	*<35* (n=157)	*35–70* (n=2)	*>70* (n=0)	*<35* (n=1)	*35–70* (n=12)	*>70* (n=37)
3×3	0.61	0.79	0.84	0.62	1.00	0.00	0.00	0.75	0.84
5×5	0.42	0.71	0.76	0.43	1.00	0.00	0.00	0.67	0.76
7×7	0.20	0.36	0.70	0.20	0.50	0.00	0.00	0.33	0.70
SVR	0.59	0.79	0.78	0.60	1.00	0.00	0.00	0.75	0.78
SB	0.55	0.79	0.84	0.55	1.00	0.00	0.00	0.75	0.84

break are computed for each pixel and are applied as a unique window size for that location. In the simulated panchromatic channel LM filtering with a variable window size determined by the semivariance method correctly located 64% of the trees in the entire stand, and resulted in a commission error of 19% (Table 5). The lack of a consistent improvement in comparison to the fixed window LM filtering is likely due to the selection of small window sizes from the same image spatial features that result in local maxima being found where no trees are present. Instead of a poorly fit window identifying spurious local maxima and resulting in a high commission level, variable-sized windows are being generated for the false positives. The LM generated from slope breaks have fewer false positives than those from the semivariance range. The measurement of slope breaks from the imagery appears more sensitive to the actual extent of the crown. The semivariance range values, at the study image spatial resolution of 1 m, have a greater likelihood of generating stand level information rather than individual crown information and are thus less locally adaptive.

Distribution of Error

At the 1-m spatial resolution, an object resolution exists that precludes the locating of smaller trees with LM filters. Yet, if the larger trees in the stand are consistently located, it may be possible to account for most of the stand basal area. In this section we address the distribution of omission and commission in terms of the LM detection technique and tree DBH.

The relationship between DBH and stand age is strong (Table 1, Fig. 3). Within each stand age component there is a range of DBH values that allows for the investigation of tree-size thresholds for detection of trees with an LM filter. The trees with DBHs larger than 35 cm are found more readily (Table 6). The fixed window-size LM filters were most successful in locating trees of DBH less than 35 cm, although the variable-size windows were almost as effective. However, the relative success in finding the larger trees may be more important since the trees with DBH greater than 35 cm account for most of the basal area within a stand. The commission error increases the number of trees that are identified, resulting in erroneous results and an inability to use the LM-identified trees for further analysis, such as input data for the estimation of basal area.

Estimation of Basal Area

Basal area is the combined surface area of wood at breast height, and is often estimated to provide an indication of tree volume in a particular area. Do our results in locating trees with LM filtering allow us to accurately estimate basal area? Stand basal area in m^2 may be estimated from a mean stand DBH and an estimated number of stems; the mean of field-measured DBH values from a summary field sample can be input to a basal area equation to provide a mean basal area value of an individual tree within a homogeneous area. In an operational context, a field sampling procedure to characterize the variability in a forest area would be undertaken to generate representative inventory values for extrapolation with digital remotely sensed stem counts. The stem counts derived from the LM filtering can then be used to extrapolate the mean tree basal area over the specified area.

In the present case, the mean stand basal area is known and is based on field-measured values from the plantation and mature strata. This measured value may be compared to estimates made from expected DBH values combined with LM stem counts. For the plantation and mature strata the basal area is computed based on the arithmetic mean DBH values as measured in the field and LM stem counts. The basal area of the entire study area is summed from the plantation and mature values (Table 7). The disparity between the plantation and mature mean DBH values measured in the field precludes the estimation of an overall basal area value from a mean DBH. The total basal area estimated from the stand means compares favorably to the actual basal area computed from the field-measured DBH values (Table 7). As the basal area estimated from the mean DBH closely approximates the field-measured basal area, we may address the implications of estimating basal area from LM generated stem counts.

Table 8 shows the basal area estimates for the entire study area (all) and broken down by stand age (plantation and mature), illustrating the effect of the distribution of errors by DBH. Also illustrated is the potential confusion in results created by the inclusion of false-positive LM in subsequent computations. In an operational

Table 7. Summary Basal Area Values, in m^2, Computed from Actual Field Data and Mean Values for Plantation and Mature Strata, with Basal Area for Entire Stand Area Summed from Plantation and Mature

	All (n=*209*)	*Plantation* (n=*159*)	*Mature* (n=*50*)
BA from actual field-measured DBHs	36.7463	6.3061	30.4402
BA from mean DBHs	34.6946	6.3219	28.3726
Mean BA per tree	–	0.03976	0.56745

$BA=0.00007854 \cdot DBH^2$. Plantation mean DBH=22.5 cm, mature mean DBH=85.0 cm. Basal area formula from Husch, et al. (1973), p. 100.

forest management exercise, the difference between correct and false-positive local maxima would be unknown. As a result, the number of stems utilized for computations would be that presented here as total LM. In Table 8 we present the percentage of basal area accounted for by all LM-indicated trees, correct trees, false positives, and missed trees. To ascertain the proportion of actual basal area accounted for with each LM filter, for plantation and mature the basal area is estimated from the mean values multiplied against the number of stems indicated with the LM filter as the total of correct and false positives. To represent the entire study area, the results from plantation and mature are summed. To compute the total basal area accounted for with LM, the basal area computed based on the total LM is divided by the basal area expected for the mean DBH values (presented in Table 7). As a result, for plantation and mature the basal area accounted for with LM is equal to the proportion of total LM, including false positives, over the total number of possible stems. For the entire study area, variability between the total LM proportion and the basal area accounted for with LM is evident, which is based on the variable contributions of the plantation and mature stands to compute a total basal area value.

The results for the basal area estimation from mean DBH values and LM filter-identified stems (Table 8) are presented in terms of LM filtering technique on the panchromatic spectral data and stand age. The results for the 3×3 fixed LM filter on the spectral data show that 141% of the basal area is accounted for, as a consequence of the overestimation of basal area for the mature stand. The underestimation of the plantation trees (67%) is made up for by an overestimation of the mature trees (158%) resulting in the overestimation of the basal area present. The commission error for the mature trees, with almost as many false positives as correct trees, causes the overestimation. The lower commission error present for the variable-sized window on the panchromatic spectral channel results in a smaller proportion of the total basal area as a result of false positives; therefore, providing a preferred result (107% overall, 59% plantation, and 1.18% mature). The count accuracy of the variable window size based on slope breaks on the panchromatic spectral channel is lower (recall Table 5), yet the lower commission error provides a more precise basal area result.

This example illustrates that the desired use of the LM-identified stems will dictate the interpretation of the success or failure of a particular LM filtering technique. The object-resolution relationship with 1-m spatial resolution data has influenced the unique results presented here. If the larger trees are being found with LM filters and these large trees account for most of the basal area present, LM filtering may be useful. If LM filtering is useful for finding the larger trees, how large must these trees be?

Effect of Crown Radius

For a given spatial resolution, bigger trees are easier to locate because they are represented with a higher number of pixels than small trees. An understanding of the threshold tree size for detection at a particular resolution

Table 8. Basal Area Estimation from Mean DBH by Stand Age for Two LM Filters Processing Panchromatic Data

	All		*Plantation*		*Mature*	
	n	%	n	%	n	%
Fixed window size (3×3)						
Total	186	89.0	107	67.3	79	158.0
Correct	139	66.5	99	62.3	40	80.0
False positive	47	22.5	8	5.0	39	78.0
Missed	70	33.5	60	37.7	10	20.0
BA accounted for		141.5		67.3		158.0
Variable size window (SB)						
Total	153	73.2	94	59.1	59	118.0
Correct	129	61.7	89	56.0	40	80.0
False positive	24	11.5	5	3.1	19	38.0
Missed	80	38.3	70	44.0	10	20.0
BA accounted for		107.3		59.1		118.0

Table 9. Proportion of Trees Identified with the LM Filters in the Panchromatic Range by Crown Radius Range (n=209)

	0 m to 1 m (n=*6*)	*1 m to 1.5 m* (n=*76*)	*1.5 m to 2 m* (n=*71*)	*2 m to 3 m* (n=*27*)	*3 m to 4 m* (n=*25*)	*>4 m* (n=*4*)
Fixed window size						
3×3	0.33	0.51	0.73	0.89	0.76	0.75
5×5	0.33	0.32	0.49	0.85	0.72	0.75
7×7	0.17	0.13	0.25	0.59	0.60	0.75
Variable window size						
SVR	0.33	0.50	0.69	0.89	0.72	0.75
SB	0.33	0.43	0.68	0.89	0.76	0.75

is important for the application of LM filters. For the object resolution present in this study a relationship exists between the individual crown size and the likelihood of the identification of a particular tree with an LM filter.

In Table 9 we present the proportion of trees found by each LM filter in a series of crown radius classes. The crown radii values may be converted to areas to allow for an indication of how many pixels may be the result of a particular tree. The break between the radius classes below and above 2 m corresponds to a rough division between the plantation and mature stand. As a result, Table 9 may be interpreted in terms of crown radii or by age classes (which correspond to ranges of crown size). The success rates based on tree crown size in Table 9 should be interpreted with the commission error (Table 5) in consideration of overall levels of LM filter success.

In Table 9 we also present the proportion of trees found by each LM filter for the panchromatic spectral channel. Assessment of the levels of success at each window size for the fixed LM filtering of the spectral data provide an indication of the relationship between tree crown size and image spatial resolution, or the object resolution. For example, consider the fixed filter on the panchromatic image data; the change in the proportion of trees found with the 3×3, 5×5, and 7×7 pixel windows indicates the size of the image spatial domain created by a given tree crown size. Half the trees with a crown radius of 1 m to 1.5 m are found with a 3×3 LM filter, yet only 32% and 13% of the trees are found with 5×5 and 7×7 pixel windows, respectively. At the next larger radius class, 1.5 m to 2 m, the pattern of decreasing success with increasing window size holds, but the proportions of success increase. As the tree crown radii continue to increase, the variability in the magnitude of the success proportions decreases. The increased stability of the success proportions is due to all window sizes being able to encompass the spatial region of imagery representing a particular tree crown. The proportion of trees that are found by the variable window-size LM filters are similar to those of the fixed window size. Lower commission error is the chief advantage of the variable window-size filters.

In our study, the key threshold of crown radius for successful identification of a tree using LM filters appears to be 1.5 m for both fixed and variable window sizes. Trees smaller than 1.5 m may be successfully located, but not as reliably. These generalizations are applicable for the object-resolution relationship existing between the 1-m spatial resolution image data and the field data under consideration.

CONCLUSIONS

The use of local maxima filters on high spatial resolution remotely sensed imagery to identify the locations of trees is a simple methodology. In question is the accuracy of the various local maxima filtering approaches available. Fixed and variable window sizes are compared, with the number of correct trees found to be quite similar, yet the number of wrongly identified trees is greater in the case of the fixed window sizes. As a result, the chief concern with local maxima filtering appears to be the reduction of commission error, or false positives. A 3×3 filter will find all the trees that may be identified in the imagery, yet many trees are also wrongly indicated. The variable window-size technique allowed for a reduction in commission error, or identification of false positives.

The trade-off between total proportion of trees correct and the level of commission error allows the user to determine which is more important, based on the intended use of the LM filter-generated tree locations. The presentation of a process to estimate basal area from the LM filter-generated tree locations demonstrated that slightly lower proportions of successful stem identification may be quite acceptable since the majority of basal area is accounted for by large trees, and achieving a minimum of commission error is more important.

The image spatial resolution necessary for locating stems on digital remotely sensed image data will vary based on the relationship between the spatial resolution and the tree crown-size distribution. In this study, the key crown-size threshold for successful identification using LM filters is at 1.5-m crown radius. Trees smaller than this threshold may be successfully located, but at a lower rate of success. These generalizations are applicable for the object-resolution relationship present be-

tween the 1-m spatial resolution image data and the unique field data under consideration. These results may influence the desired image spatial resolution of subsequent studies of coniferous forests based on knowledge of the mean tree-size distributions under consideration.

While much potential has been shown in forest investigations with submeter spatial resolution data, this research addresses the potential of 1-m spatial resolution panchromatic data, similar to that of high spatial resolution satellite sensors. With the panchromatic satellite sensors with a spatial resolution of 1 m, for coniferous trees with crown radii of less than 1.5 m, low success rates for LM filtering results should be anticipated. For trees larger than the threshold values, moderate success may be anticipated. Image fusion with the lower spatial resolution multispectral information available on the satellites, on the order of 4 m, will allow for the incorporation of multispectral data to aid in high spatial resolution analyses of forests.

Based on the findings presented in this study, future research directions include the development of an index relating the necessary object-resolution relationship necessary for stem identification with LM filters, LM filtering of imagery of different resolutions, and the creation of different methods to reduce commission error based on spectral thresholds and/or contextual information.

The authors wish to express their gratitude to Geoff Hay, who rigorously collected the field data utilized in this study, and Gordon Joyce of the Greater Victoria Watershed District Office for permitting us to conduct research in the watershed. The efforts of Laurie Miller on subsequent field data validation efforts are appreciated. Nigel Daley and Charles Burnett are also thanked for assistance in computer programming and the interpretation of initial results. Dr. François Gougeon of the Canadian Forest Service is thanked for valuable comments and suggestions. Two anonymous reviewers are also thanked for many excellent comments and suggestions that improved this final manuscript.

REFERENCES

Aplin, P., Atkinson, P., and Curran, P. (1997), Fine spatial resolution satellite sensors for the next decade. *Int. J. Remote Sens.* 18(18):3873–3881.

Barbezat, V., and Jacot, J. (1999), The CLAPA project: Automated classification of forest with aerial photographs. In *Proceedings of the International Forum on Automated Interpretation of High Spatial Resolution Digital Imagery for Forestry*, Victoria, BC, Feb. 10–12, 1998, Natural Resources Canada, Canadian Forest Service, Pacific Forestry Centre, pp. 345–356.

Brandtberg, T. (1997), Towards structure-based classification of tree crowns in high spatial resolution aerial images. *Scand. J. For. Res.* 12:89–96.

Culvenor, D., Coops, N., Preston, R., and Tolhurst, K. (1999), A spatial clustering approach to automated tree crown delineation. In *Proceedings of the International Forum on Automated Interpretation of High Spatial Resolution Digital Imagery for Forestry*, Victoria, BC, Feb. 10–12, 1998, Natural Resources Canada, Canadian Forest Service, Pacific Forestry Centre, pp. 67–80.

Curran, P., and Atkinson, P. (1998), Geostatistics and remote sensing. *Prog. Phys. Geog.* 22(1):61–78.

Daley, N., Burnett, C., Wulder, M., Niemann, K., and Goodenough, D. (1998), Comparison of fixed-size and variable-sized windows for the estimation of tree crown position, *Proc. IGARSS '98*, Seattle, WA, USA, July 6–10, pp. 1323–1325.

Dralle, K., and Rudemo, M. (1997), Stem number estimation by kernel smoothing of aerial photos. *Can. J. For. Res.* 26:1228–1236.

Franklin, S. (1994), Discrimination of subalpine forest species and canopy density using digital CASI, SPOT PLA, and Landsat TM data. *Photogramm. Eng. Remote Sens.* 60 (10):1233–1241.

Franklin, S., Wulder, M., and Lavigne, M. (1996), Automated derivation of geographic windows for use in remote sensing digital image analysis. *Comp. Geosci.* 22(6):665–673.

Goodenough, D., Charlebois, D., Matwin, S., and Robson, M. (1994), Automating Reuse of Software for Expert System Analysis of Remote Sensing Data, *IEEE Transact. Geosci. Remote Sens.* 32(3):525–533.

Goodenough, D. G., Charlebois, D., Bhogal, A. S., and Matwin, S. (1997), Automated forest inventory update with SEIDAM, *Proc. IGARSS'97*, Singapore, pp. 670–673.

Gougeon, F. (1999), Automatic individual tree crown delineation using a valley-following algorithm and a rule-based system. In *Proceedings of the International Forum on Automated Interpretation of High Spatial Resolution Digital Imagery for Forestry*, Victoria, BC, Feb. 10–12, 1998, Natural Resources Canada, Canadian Forest Service, Pacific Forestry Centre, pp. 11–23.

Gougeon, F. A., and Moore, T. (1988), Individual tree classification using MEIS-II imagery. In *Proc. 1988 Intl. Geoscience and Remote Sensing Symposium (IGARSS'88)*, Edinburgh, Scotland, September 13–16, pp. 927.

Gougeon, F. A., Moore, T. (1989), Classification individuelle des arbres à partir d'images à haute résolution spatiale. In *Télédétection et Gestion des Ressources*, (M. Bernier, et al., Eds.), Vol. VI—6e Congrès de L'Association Québécoise de Télédétection, Sherbrooke, Québec, Canada, May 4–6, pp. 185–196.

GVWD (Greater Victoria Water District), (1991), *Greater Victoria Water District Watershed Management Forest Cover Classification, Sooke Lake Watershed, Scale 1:10,000.* Prepared by Hugh Hamilton, Ltd., Vancouver, BC.

Hay, G., and Niemann, K. (1994), Visualizing 3-D texture: A three-dimensional approach to model forest texture. *Can. J. Remote. Sens.* 20(2):89–101.

Husch, B., Miller, C., and Beers, T. (1972), *Forest Mensuration*, Ronald Press Company, New York.

Jupp, D., Strahler, A., and Woodcock, C. (1988), Autocorrelation and regularization in digital images: I. Basic theory, *IEEE Transact. Geosci. Remote Sens.* 26(4):463–473.

Lévesque, J., and King, D. (1996), Semivariance analysis of tree crown structure in airborne digital camera imagery. In *Proc. 26th Int. Symp. Rem. Sens. Env./18th Canadian Symp. Rem. Sens.*, Vancouver, BC, March 23–26, pp. 275–278.

Mangold, R., (1999). IKONOS has arrived, *EOM* 8(9): 7.

Matheron, G. (1963), Principles of geostatistics. *Econ. Geol.* 58:1246–1266.

Niemann, K. O., Adams, S., and Hay, G. (1999), Automated tree crown identification using digital orthophoto mosaics. In *Proceedings of the International Forum on Automated Interpretation of High Spatial Resolution Digital Imagery for Forestry*, Victoria, BC, Feb. 10–12, 1998, Natural Resources Canada, Canadian Forest Service, Pacific Forestry Centre, pp. 105–113.

Pinz, A. (1999), Tree isolation and species classification. In *Proceedings of the International Forum on Automated Interpretation of High Spatial Resolution Digital Imagery for Forestry*, Victoria, BC, Feb. 10–12, 1998, Natural Resources Canada, Canadian Forest Service, Pacific Forestry Centre, pp. 127–139.

Pollock, R. (1999), Individual tree recognition based on a synthetic tree crown image model. In *Proceedings of the International Forum on Automated Interpretation of High Spatial Resolution Digital Imagery for Forestry*, Victoria, BC, Feb. 10–12, 1998, Natural Resources Canada, Canadian Forest Service, Pacific Forestry Centre, pp. 25–34.

Strahler, A., Woodcock, C., and Smith, J. (1986), On the nature of models in remote sensing. *Remote Sens. Environ.* 20: 121–139.

Till, S., McColl, W., and Neville, R. (1983), Development, field performance and evaluation of the MEIS-II multi-detector electro-optical scanner. Presented at the *Seventeenth International Symposium on Remote Sensing of Environment*, Ann Arbor, Michigan, May 9–13, pp. 1137–1146.

Warner, T., Lee, J., and McGraw, J. (1999), Delineation and identification of individual trees in the eastern deciduous forest. In *Proceedings of the International Forum on Automated Interpretation of High Spatial Resolution Digital Imagery for Forestry*, Victoria, BC, Feb. 10–12, 1998, Natural Resources Canada, Canadian Forest Service, Pacific Forestry Centre, pp. 81–91.

Wu, Y., and Strahler, A. (1994), Remote estimation of crown size, stand density, and biomass on the Oregon transect. *Ecol. Applic.* 4(2):299–312.

Wulder, M. (1998), Optical remote sensing techniques for the assessment of forest inventory and biophysical parameters. *Prog. Phys. Geog.* 22(4):449–476.

Wulder, M. (1999), Image spectral and spatial information in the assessment of forest structural and biophysical data. In *Proceedings of the International Forum on Automated Interpretation of High Spatial Resolution Digital Imagery for Forestry*, Victoria, BC, Feb. 10–12, 1998, Natural Resources Canada, Canadian Forest Service, Pacific Forestry Centre, pp. 267–281.

Wulder, M., LeDrew, E., Franklin, S., and Lavigne, M. (1998), Aerial image texture information in the estimation of northern deciduous and mixed wood forest leaf area index (LAI). *Remote Sens. Environ.* 64:67–76.